Energy Storage Materials 23 (2019) 261–268

Contents lists available at ScienceDirect

Energy Storage Materials

journal homepage: www.elsevier.com/locate/ensm

Engineering stable electrode-separator interfaces with ultrathin conductive polymer layer for high-energy-density Li-S batteries

Yuanjian Li [a], Wenyu Wang [a], Xiaoxiao Liu [a], Eryang Mao [a], Mintao Wang [a], Guocheng Li [a], Lin Fu [a], Zhen Li [b], Alex Yong Sheng Eng [c], Zhi Wei Seh [c], Yongming Sun [a,*]

[a] *Wuhan National Laboratory for Optoelectronics and School of Optical and Electronic Information, Huazhong University of Science and Technology, Wuhan, 430074, China*

[b] *State Key Laboratory of Material Processing and Die & Mould Technology School of Materials Science and Engineering, Huazhong University of Science and Technology, Wuhan, 430074, China*

[c] *Institute of Materials Research and Engineering, Agency for Science, Technology and Research (A*STAR), 2 Fusionopolis Way, Innovis, 138634, Singapore*

ARTICLE INFO

Keywords:
Lithium-sulfur batteries
Electrode-electrolyte interface
Conductive polymer
Lithium metal

ABSTRACT

Lithium-sulfur (Li-S) battery has been regarded as a promising energy-storage system due to its high theoretical specific capacity of 1675 mAh g^{-1} and low cost of raw materials. However, several challenges remain to make Li-S batteries viable, including the shuttling of soluble lithium polysulfide intermediates and pulverization of Li metal anode. Engineering stable electrode-separator interfaces without causing large mass/volume increase of inactive materials and electrolyte uptake is an effective approach to improve the cycling stability of Li-S batteries while maintaining high available energy density. Herein, we report the engineering of a stable electrode-separator interface with an ultrathin conductive polymer nanolayer on the pore walls of both surfaces of the separator via a simple and scalable approach using *in-situ* vapor-phase polymerization of polypyrrole (PPy) on commercial Celgard separator with only a small increase in overall mass and volume. The inherent hydrophilicity of PPy enables the separator to have enhanced electrolyte uptake, which facilitates homogenous Li^{+} flux and thus uniform plating and stripping of metallic lithium at the anode side during the charge/discharge processes. Meanwhile, the chemical immobilization effect of PPy suppresses the migration of the soluble polysulfides and improves the stability of the sulfur cathode. We showed that a Li||Li symmetrical cell with the PPy modified separator gave a low and stable overpotential of less than 30 mV for over 250 h' stripping and plating test at 1 mA cm^{-2} with a fixed areal capacity of 3 mAh cm^{-2}, which was significantly better than that using a regular Celgard separator. Using the PPy modified separator, Li-S cell with sulfur/carbon black composite cathode and lithium anode delivered stable cycling for 250 cycles at 0.5 *C* with a low capacity decay rate of 0.083% per cycle. Even for a Li-S cell with a high-areal-capacity sulfur cathode (4.8 mAh cm^{-2}), good cycling stability was achieved. It gave a reversible areal capacity of 3.6 mAh cm^{-2} after 150 charge/discharge cycles at 0.2 *C* with 75.6% capacity retention. Besides, the as-achieved separator showed better thermal stability than the bare counterpart. This work offers an alternative approach for achieving a practical Li-S battery toward high energy density and long cycle life through simple and scalable separator-electrode interface engineering without significant increase in volume and mass.

1. Introduction

Lithium-ion batteries are an important power source and have dominated portable electronics [1,2]. Nonetheless, the development of advanced energy-storage battery technology systems beyond conventional lithium-ion batteries is critical for various high demand energy storage applications such as electric vehicles and grid-level storage [3,4]. Among various battery systems, Li-S battery has been regarded as one of the most promising candidates for future-generation energy storage devices, due to its inherently high theoretical energy density (2600 Wh kg^{-1}) and low cost of raw materials [5,6]. However, the commercialization of Li-S battery is still hindered by the intractable challenges from the sulfur cathode and lithium metal anode. One critical problem is the parasitic shuttling behaviors of the soluble intermediate polysulfides,

---

* Corresponding author.
E-mail address: yongmingsun@hust.edu.cn (Y. Sun).

https://doi.org/10.1016/j.ensm.2019.05.005
Received 30 March 2019; Received in revised form 1 May 2019; Accepted 4 May 2019

which leads to poor Coulombic efficiency and quick capacity degradation [7–9]. Another big problem is the corrosion of the lithium metal anode. The inhomogeneous plating/stripping of metallic lithium and the high reactivity of lithium metal result in the quick consumption of electrolyte, formation of the so-called "dead Li" (inactive Li), and violent safety hazard of such batteries [10–12].

To overcome the aforementioned issues and achieve enhanced electrochemical performance of Li-S batteries, various approaches have been explored, including electrolytes engineering [13,14], functionalization of separator [15,16], and rational design of advanced sulfur host materials [17,18]. Among these, Li-S batteries with modified separators or interlayers take the approach of blocking the diffusion of soluble intermediate polysulfides from the cathode side to the anode side, presenting exciting progress [19–21]. Till now, a wide variety of materials have been employed to build modified separators or interlayers and create functional separator-electrode interfaces for Li-S batteries, including carbon-based materials [22–24], hydrophilic polymers [25–27], inorganic metal compounds [28–30], and their composites [31–33]. Typically, a carbon paper (CP) as interlayer between the cathode and regular separator and a carbon black layer modified separator were successfully used to suppress the diffusion of polysulfides and enhancing electrochemical performance [34,35]. At the anode side, improved lithium plating/stripping behavior was achieved by using separators coated with functional materials [36,37]. As an example, a polydopamine coating layer on polyethylene separator enabled good distribution of Li ionic flux over the lithium metal anode and suppressed the growth of Li metal dendrites [38]. Despite of the progress, several issues still exist for real applications of Li-S batteries: (1) Few reports demonstrated the design of functional separators/interlayers aiming at addressing the challenges of both the sulfur cathode and lithium metal anode concurrently [39–41]. Improved electrochemical performance was mainly achieved from either the improved sulfur cathode side or the lithium metal anode side. (2) The main approaches for the modification of separators or preparation of interlayers were vacuum filtration [42,43] and slurry coating [44,45]. These approaches were complicated, especially for double side coating/modification for improving both the cathode and anode, and not suitable for large-scale manufacturing. (3) The modification of separators often introduced a substantial amount of inert materials, especially for using individual interlayers or thick functional coating layers, which, together with the consequently increased liquid electrolyte uptake, significantly decreased the practical energy density of Li-S batteries [38,46]. Thus, it is highly desirable yet challenging to develop a simple and scalable route to prepare an ultrathin, lightweight (e.g., $<0.2\,\mu m$, $< 0.2\,mg\,cm^{-2}$) functional layer of separators aiming to improve the electrode-separator interface and enhance the battery performance at both the cathode and anode sides for practical high energy density Li-S batteries.

Herein, we report an *in-situ* vapor-phase polymerization approach to generate an ultrathin, lightweight bifunctional polypyrrole (PPy) modification layer on commercial Celgard separator and construct improved electrode-separator interfaces for Li-S batteries, which realizes both stable sulfur cathode and lithium metal anode due to the multiple advantages. First, the hydrophilic surface of polypyrrole enhances the electrolyte wettability and enables uniform Li ionic flux, leading to uniform lithium metal plating and stripping at the anode side. Second, the unique structure and functional groups of PPy provides favorable chemical affinities to immobilize polysulfides and suppresses their shuttle effect. Meanwhile, the conducting polymer layer facilitates upper electron transportation and their redox reactions at the sulfur cathode. Third, the synthesis is simple and scalable, and is suitable as a method to modify both sides of the separator in a single step. Lastly, the lightweight and ultrathin layer of PPy minimizes the energy density loss for high performance Li-S batteries. With these merits, we show that a Li||Li symmetrical cell with such functional separator sustained stable Li plating/stripping cycling test over 250 h with a fixed capacity of $3\,mA\,h\,cm^{-2}$ at $1\,mA\,cm^{-2}$ and exhibited low overpotential of less than 30 mV upon cycling. Paired with a PPy modified separator, a Li-S cell delivered stable cycling for 250 cycles at 0.5 *C* with a low capacity decay rate of 0.083% per cycle. Moreover, the capacity retention of a Li-S cell with a high-areal-capacity sulfur cathode ($4.8\,mAh\,cm^{-2}$) was 75.6% after 150 charge/discharge cycles at 0.2 *C*.

2. Results and discussion

Fig. 1a illustrates the formation of PPy functional layer on the surface of Celgard separators. A Celgard 2400 separator was firstly soaked into a $FeCl_3$ ethanol solution for catalyst loading and then placed in the vapor of pyrrole monomer for *in situ* vapor-phase polymerization [47]. After reaction, an ultrathin PPy nanolayer was uniformly formed on the pore walls of both surfaces of the separator. It is noted that such a fabrication approach is scalable. In our experiment, a PPy modified separator with a size of 23 cm × 6 cm was easily prepared (Fig. 1b). A peel test was performed and the result demonstrated the good adhesive strength between the PPy functional layer and the separator (Figs. S1a–d). Moreover, a piece of PPy modified separator was folded and crumbed and it recovered its initial state after the release of strain without the peeling of the PPy layer (Figs. S1e–h). Therefore, the PPy functional layer is mechanically durable and adhered to the separator firmly. The morphologies of the separators with and without PPy modification were characterized by scanning electron microscopy (SEM). The pristine separator exhibited abundant nanopores with a size of ~100–200 nm (Fig. 1c). Slight shrinkage with 30–50 nm in pore size was observed for these nanopores after the PPy coating (Fig. 1d), while the overall pore structure is well-preserved. The thickness of the PPy coating layer on the pore walls of the separator was 15–25 nm calculated based on the cross-section SEM images before and after modified by PPy coating (Fig. 1d). The mass loading of the PPy layer is only $\sim 0.13\,mg\,cm^{-2}$, and the thickness of the PPy modified layer of the separator is ~65 nm on average calculated based on the density of PPy, and assuming a dense structure. The real thickness of this modified layer is slightly thicker due to the porous structure. Nonetheless, the mass and the thickness of the PPy layer are much less than that of various separator coating layers or interlayers in previous studies, as shown in Fig. 1e. Ultrathin and lightweight functional coating is of crucial importance in improving the cycling stability of Li-S batteries while maintaining their superiority in energy density. X-ray photoelectron spectroscopy (XPS) was performed for the separators with and without PPy modification. A new N 1s peak at 399.8 eV appears after PPy coating (Fig. 1f). The high-resolution N 1s spectrum (Fig. 1g) suggests the existence of three typical nitrogen species of –N= (399.6 eV), –N– (400.7 eV), and N^+ (401.7 eV) motifs, arising from the PPy [47,48]. These nitrogen heteroatoms provide strong chemical adsorption sites for polysulfides and thus suppress their migration from the cathode to anode side [49,50]. Moreover, the hydrophobic surface of separator turns hydrophilic after PPy modification due to the intrinsic hydrophilicity of PPy. Fig. S2 shows the comparison of the electrolyte wettability of two separators. A 50 μL electrolyte droplet spreads rapidly on the PPy modified separator while it maintains its sharp on the pristine separator. The corresponding contact angles between the separators and electrolyte are ~37° and ~9°, respectively (Fig. S2). The results suggest that the electrolyte wettability of the separator is greatly improved after the PPy modification. As a result, the capability of electrolyte uptake of the separator increases from 70% to 108%, which facilitates Li-ion diffusion through the separator [26,38]. Besides, the thermal stability of the separator is significantly improved after PPy coating. The separators with and without PPy coating were treated at 150 °C for 10 min. A 48% shrinkage in size was observed for the pristine Celgard separator. In contrast, the shrinkage of the PPy modified separator was only 12%. (Fig. S2). The SEM images of Celgard separator with and without PPy modification after the thermal treatment were investigated to further confirm the effect of PPy layer on the thermal stability of the separators (Fig. S3). After the heat treatment at 150 °C for 10 min, the collapse of the pores and cracks were observed for the pristine separator (Figs. S3a and

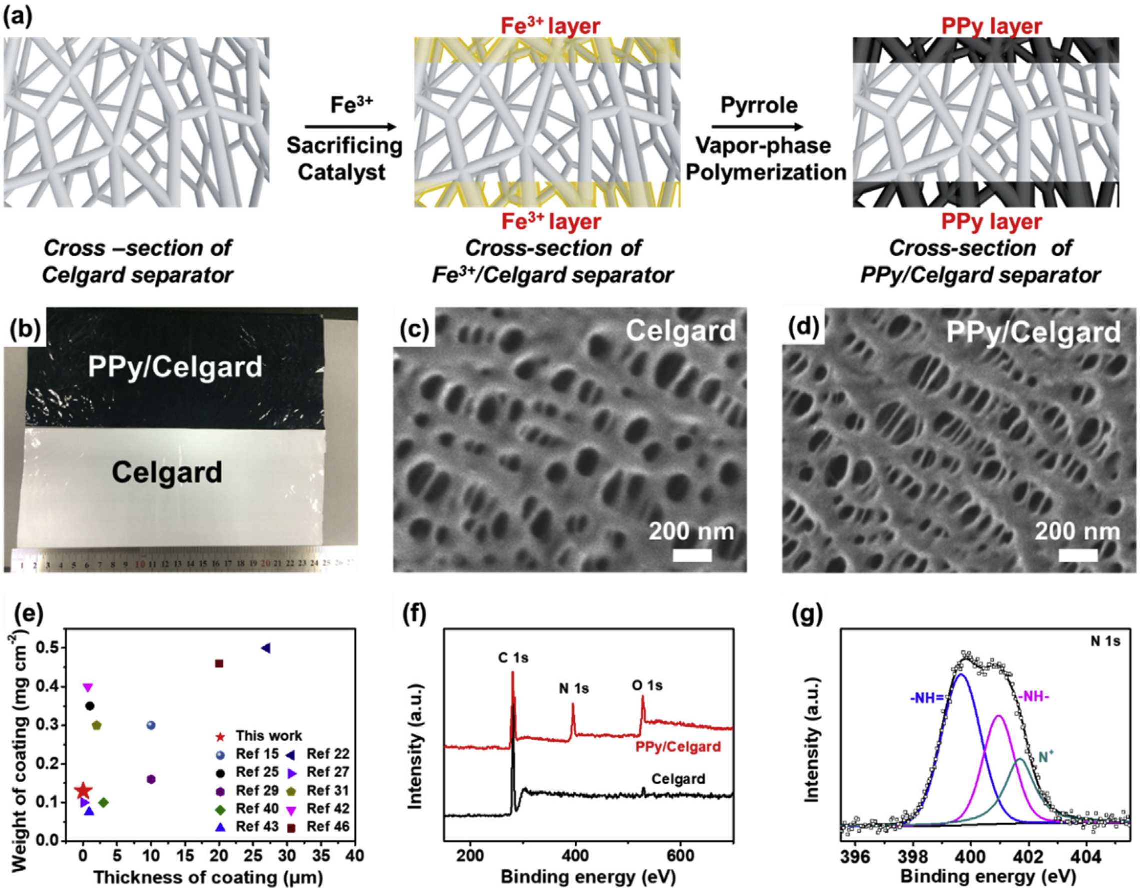

Fig. 1. (a) The schematic illustration of coating a PPy ultrathin nanolayer on both surfaces of the separator using a facile vapor-phase polymerization process. (b) Digital photos of the Celgard separator without and with PPy modification. Top-view SEM images of a Celgard separator (c) without and (d) with PPy modification. The size of the nanopores of the separator was reduced after PPy modification. (e) Comparison of the thickness and weight of functional coating on the Celgard separator in this work with those reported in the literature. (f) XPS spectra of a Celgard separator without and with PPy modification. The signal of N arises from the PPy modification layer. (g) High -resolution N 1s spectrum of the PPy modified separator.

b). In contrast, the initial structure of the PPy modified separator was well maintained (Fig.1d, Figs. S3c and d), validating the improved thermal stability due to the PPy modification. The melting point of the materials decides the thermal stability of the separator. At the melting point or higher temperature, the pores of the separator collapse and the separator shrinks [51]. Celgard 2300 membranes with a polypropylene/polyethylene/polypropylene (PP/PE/PP) trilayer structure are used as the separator for batteries in this work. The melting points are 130 °C and 165 °C for PE and PP, respectively. Thus, the pristine separator shrinks after its heat treatment at 150 °C for 10 min. Compared to PE and PP, PPy has a much higher melting point (>300 °C) and it sustains its physical strength up to 200 °C [52]. For the PPy modified separator, the PPy layer mechanically holds the overall backbone of the separators, and thus the thermal stability of the PPy modified separator is improved in comparison to the pristine separator.

The effect of PPy interface layer on the suppression of polysulfide shuttle behavior was conducted through multifarious measurements. The investigation on the permeability of soluble polysulfides through different separators was conducted using a glass cell configuration. As shown in Fig. 2a, the glass cell contains two chambers isolated by a separator with the right chamber containing a colorless ether electrolyte (1 M LiTFSI + 0.2 M $LiNO_3$ in 1,3-dioxolane (DOL)/1,2-dimethoxyethane (DME) with volume ratio of 1:1) and the left chamber containing the same ether-based electrolyte with deep brown Li_2S_6 catholyte. For the cell using a regular Celgard separator, the quick color change was observed for the electrolyte in the right chamber. It turned from colorless to light yellow after 5 min and then to yellow-brown after 24 h, suggesting the easy diffusion of polysulfides through the regular Celgard separator. In sharp contrast, no obvious color change was observed for the electrolyte in the right chamber of the glass cell using a PPy modified separator after 24 h, indicating that the shuttling phenomenon of polysulfides was suppressed by the PPy interfacial layer [53].

Self-discharge phenomenon of Li-S cells with different separators was examined by monitoring open circuit voltage (OCV) after the first charge/discharge cycle at 0.1 *C* (Fig. 2b). A drastic decay in the OCV from 2.30 to 2.20 V during the period of rest between 50 and 200 h was observed for the cell with a regular Celgard separator, indicating severe self-discharge. Compared with the cell using regular Celgard separator, the cell with PPy modified separator only exhibited a small change of 0.03 V in the OCV (from 2.30 to 2.27 V) during the same rest time. Therefore, the self-discharge behavior was effectively suppressed by using the PPy modified separator [54], and suppression of the polysulfide shuttle effect was confirmed.

Electrochemical impedance spectroscopy (EIS) tests were employed to measure the lithium ionic conductivity of different separators wetted by liquid electrolyte using a stainless steel||stainless steel (SS||SS) cell configuration with liquid electrolyte wetted separator. The Nyquist plots in Fig. 2c exhibited that the cell with PPy modified separator showed lower resistance than that using regular Celgard separator (1.07 *vs.*1.38 Ω). Thus, the PPy modified separator wetted by liquid electrolyte had larger ionic conductivity than that of the regular Celgard separator (0.39 vs. 0.32 mS cm^{-1}) [28]. Moreover, the lithium ion transfer number was measured using a potentiostatic polarization method. Calculated based on the current-time curves (Fig. 2d), the lithium ion transference

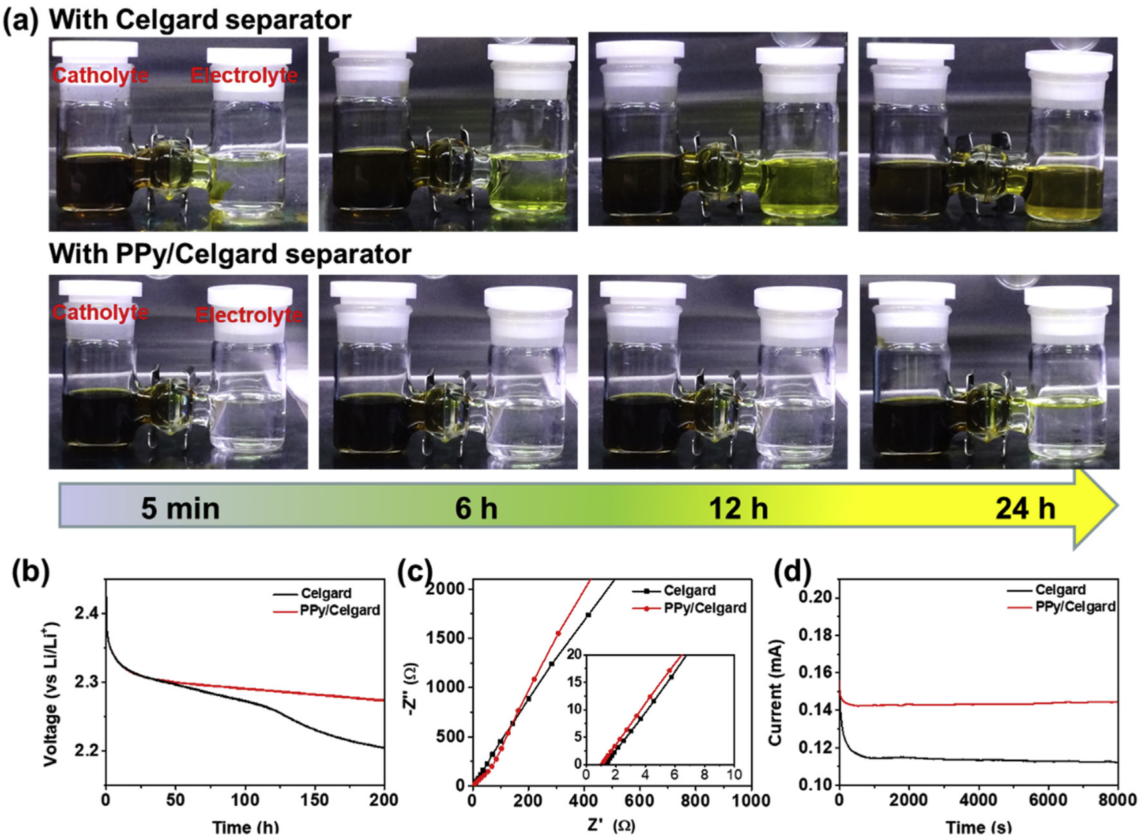

Fig. 2. (a) Optical images for the diffusion of polysulfides in glass cells with regular Celgard separator and PPy modified separator, respectively. (b) OCV versus time plot of cells using different separators. (c) Nyquist plots of SS||SS cells with liquid electrolyte wetted separators. (d) Chronoamperometry curves of Li||Li cells with liquid electrolyte wetted separators.

number were 0.47 and 0.38 for the PPy modified separator and regular separator, respectively [55]. These results demonstrate that PPy functional interfacial layer is beneficial for enhancing the lithium ion conductivity and affording fast lithium ion transfer during the charge/discharge process of batteries due to the improved electrolyte wettability.

The effect of using PPy modified separator on the electrochemical property of lithium metal electrode was investigated by constructing Li||Li symmetric cells. Fig. 3a shows the voltage profiles for cells cycling under a current density of 1 mA cm^{-2} and an areal capacity of 1 mAh cm^{-2}. Stable stripping/plating behavior with an overpotential of ~40 mV was observed for the cell with a regular Celgard separator during the initial 100 h (50 cycles) and then the overpotential of the Li||Li symmetric cell gradually increased in the following cycles and reached ~100 mV after 200 h' cycling. In contrast, the Li||Li symmetric cell using a PPy modified separator demonstrated much better cycling stability and smaller overpotential. Flat voltage plateaus with a low overpotential of ~23 mV were achieved for over 300 h' measurement (150th stripping/plating cycles). To be more specific, much improvement in voltage fluctuation was recorded for the cell using a PPy modified separator in the zoom-in voltage profiles (Fig. 3b and c), suggesting the uniform lithium ion flux caused by the functional interfacial modification of PPy [37]. Importantly, the Li||Li symmetric cell with a PPy modified separator delivered stable plating/stripping behavior at a high areal capacity of 3 mAh cm^{-2}. The overpotential maintained a low value of less than 30 mV for over 250 h' measurement (Fig. 3d). In contrast, significant increase in overpotential was observed for the Li||Li symmetric cell using a regular Celgard separator after 100 h' stripping/plating cycling at 3 mAh cm^{-2}. The improved cycling stability of the lithium metal electrode can be contributed to the enhanced electrolyte wettability, increased ionic conductivity and well-distributed Li ionic flux benefited from the functional PPy-electrode interface [56,57].

We further investigated the electrochemical performance of Li-S cells using regular Celgard separator and PPy modified separator. Fig. 4a shows the first-cycle cyclic voltammetry (CV) profiles of the Li-S cells using different separators. In the cathodic scan, two characteristic reduction peaks at ~2.27 and ~2.01 V *vs.* Li/Li$^+$ were observed for the Li-S cell with a regular Celgard separator, which corresponded to the ring-opening reduction of S_8 to soluble polysulfides Li_2S_x ($4 \leq x \leq 8$) and then to insoluble lithium sulfide (Li_2S_2/Li_2S), respectively. These two reduction peaks slightly shifted to lower overpotentials to 2.29 and 2.03 V for the Li-S cell with a PPy modified separator, the latter of which exhibited higher peak current than that with a regular Celgard separator. In the anodic sweep, one oxidation peak was observed for both cells, which could be attributed to the multistep oxidation of Li_2S_2/Li_2S to Li_2S_x ($4 \leq x \leq 8$) and finally to S_8. This oxidation peak located at 2.48 V for the Li-S cell with a regular Celgard separator and shifted to 2.43 V with increased peak current for that with a PPy modified separator. The increased peak current and the reduced redox peak potential separation indicated that faster kinetics, especially for the redox between soluble polysulfides and solid sulfur species (Li_2S_2/Li_2S), was realized by replacing regular Celgard separators with PPy functional separators. Moreover, the well-overlapped CVs in the subsequent cycles demonstrated the good electrochemical reversibility of the Li-S cell using PPy modified separators.

Galvanostatic charge/discharge measurements were performed at a constant current rate of 0.1 *C* (1 *C* = 1675 mA g^{-1}). Compared to the Li-S cell with a regular Celgard separator, the Li-S cell with a PPy modified separator exhibited smaller voltage hysteresis and delivered much higher specific capacity (1107 *vs.* 1271 mAh g^{-1}, Fig. 4b), consistent with the CV result (Fig. 4a). These results suggest that the PPy modified separator suppresses the diffusion of the soluble polysulfides and promotes the

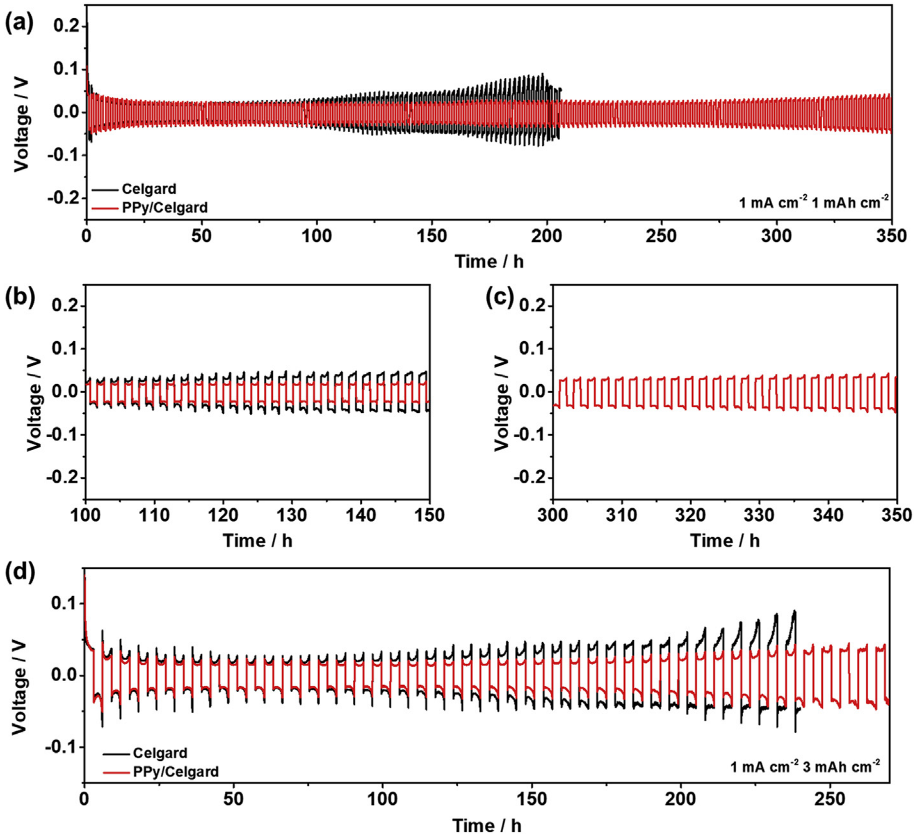

Fig. 3. Electrochemical performance of Li||Li symmetric cells. (a) Voltage profile of Li||Li symmetric cells with a regular Celgard separator and a PPy modified separator at the current density of 1 mA cm^{-2} with an areal capacity of 1 mA h cm^{-2}, and its expanded view from (b) 100–150 h and (c) 300–350 h. (d) Voltage profile of Li||Li symmetric cells with regular Celgard separator and PPy modified separator at the current density of 1 mA cm^{-2} with an areal capacity of 3 mA h cm^{-2}.

redox reaction of sulfur species, and helped to realize a high utilization of active sulfur species.

The cycling performance of Li-S cells with different separators was further tested at 0.5 *C* (Fig. 4d, e, Fig. S7). The cell with a regular Celgard separator delivered an initial capacity of 934 mAh g^{-1} that quickly degraded to 517 mAh g^{-1} after 250 cycles. Significant improvement in capacity and cycling stability was achieved for the cell using PPy modified separator by creating stable electrode-separator interfaces. With a similar initial capacity (985 mAh g^{-1}) to that using a regular Celgard separator, the capacity of the Li-S cell with a PPy modified separator remained at 805 mAh g^{-1} after 250 cycles with Coulombic efficiency of ~99.6%, demonstrating an average capacity decay rate of 0.083% per cycle, which was much lower than that of the Li-S cell using the regular Celgard separator (0.179% per cycle). Moreover, the cell with a PPy-electrode interface by using a modified separator showed stable voltage plateau with smaller voltage hysteresis than that using the regular Celgard separator during cycling (Fig. 4e and Fig. S7). Notably, the electrochemical performance of Li-S cells far outperformed many recently reported results about Li-S cells using functional separators or interlayers (Table S1), highlighting the superiority of the design of functional electrode-separator interfacial layer by using a PPy modified separator in this work. The enhanced electrochemical performance arises from combined effects of the suppression of polysulfide diffusion from the cathode to anode and improved Li-ion plating/stripping at the anode side due to the functional PPy nanolayer between the electrode and separator. The reason for enhanced electrochemical performance was further supported by the Nyquist plot achieved from the EIS (Fig. 4c). The Li-S cell with PPy modified separator delivered a much smaller charge-transfer resistance than that with a regular Celgard separator, possibly due to interaction of the polysulfides with the N-functional groups and/or higher conductivity at the PPy/polysulfide interface [26,42]. Also, stable impedance was achieved for the Li-S cell with PPy modified separator upon cycling.

Additionally, the rate capability of the Li-S battery using different separators was evaluated at various current densities ranging from 0.1 to 2 *C* (Fig. 4f and g). The Li-S cell delivered discharge capacities of 1271, 1007, 856, 770, and 682 mAh g^{-1} at 0.1, 0.2, 0.5, 1.0, and 2.0 *C*, respectively, which are higher than that of the cell with a regular Celgard separator at the same current densities (798, 850, 658, 588, and 522 mAh g^{-1}, respectively), suggesting the capability of improving the rate capability by construction of an ultrathin PPy layer between the electrode and separator. Moreover, a high reversible capacity of 907 mA h g^{-1}, 90% of the initial value, was achieved after high-current-density cycling measurement, indicating the good reversibility and stability. Furthermore, a Li-S cell with a high sulfur loading of 5.73 mg cm^{-2} was assembled and measured. As shown in Fig. 4h, the cell delivered a high initial areal capacity of 4.7 mA h cm^{-2} with a specific capacity of 834 mA h g^{-1} and maintained a high value of 3.6 mA h cm^{-2} with 75.6% capacity retention after 150 cycles. These results prove that the construction of an ultrathin PPy nanolayer between the electrode and separator can help to improve electrochemical performance of Li-S batteries even at high mass loading. Importantly, with much improved electrochemical performance, the increase in mass and volume of the entire Li-S cell was tiny and much smaller than the reported data (Table S1), due to the ultrathin (~65 nm) and lightweight (0.13 mg cm^{-2}) functional PPy interface nanolayer. Also, the ultrathin PPy nanolayer would not cause an increase of liquid electrolyte used. Thus, our strategy of using ultrathin conductive polymer interfacial layer between the separator and electrode shows great promise in practical high-energy-density Li-S batteries.

Stable structure of the Li anode and sulfur cathode on cycling is important for the electrochemical performance of Li-S batteries. We investigated the effect of PPy interfacial layer on the structure and

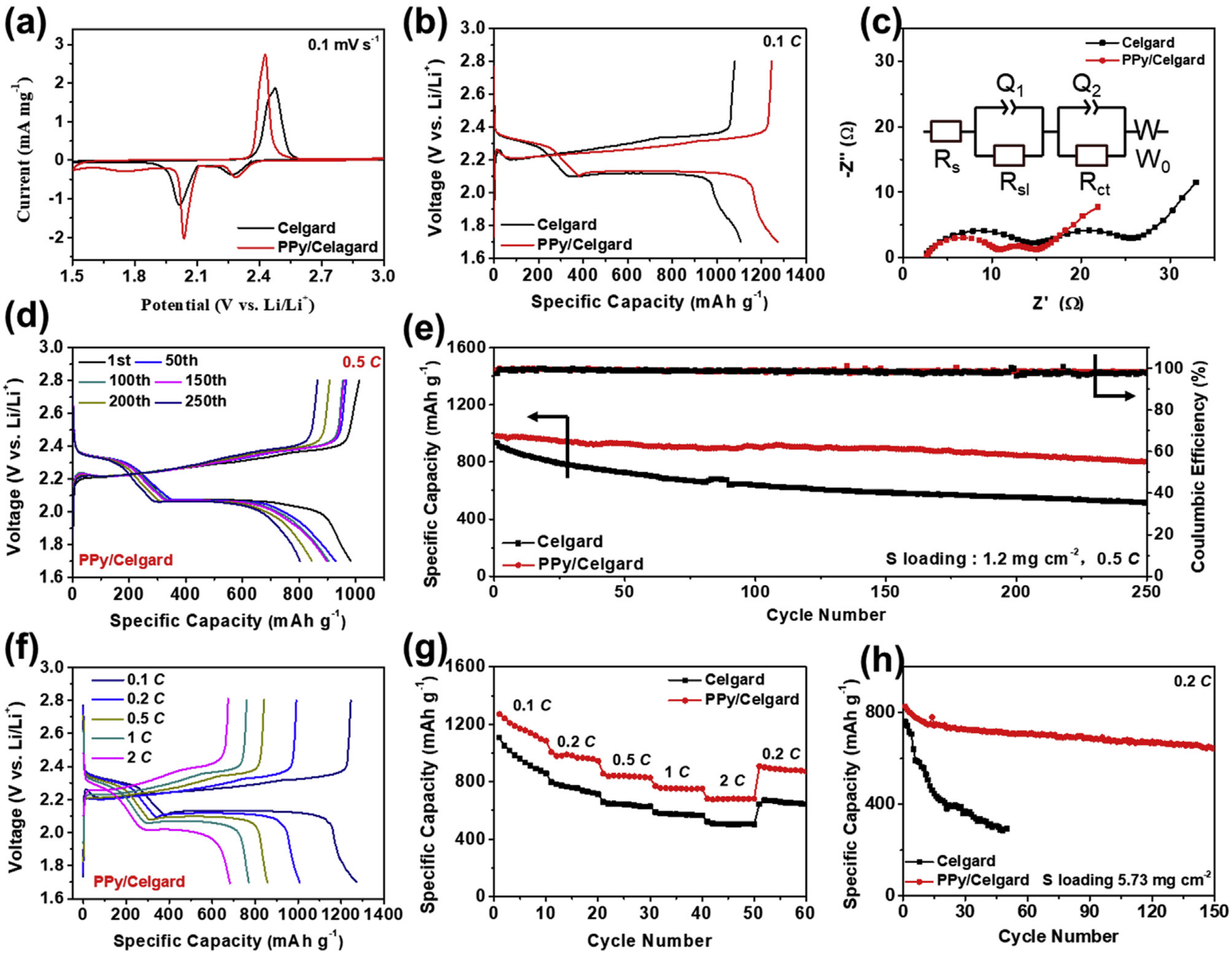

Fig. 4. Electrochemical performance of Li-S cell with a functional PPy-electrode interface. (a) CV curves at 0.1 mV s^{-1} and (b) charge/discharge curves at 0.1 *C* for Li-S cells using a regular Celgard separator and a PPy modified separator, respectively. (c) Electrochemical impedance spectra of Li-S cells with different separators. (d) Voltage-capacity plots of a Li-S cell with a PPy modified separator at 0.5 *C*. (e) Cycling performances of Li-S cells with different separators at 0.5 *C* with sulfur loading of 1.2 mg cm^{-2}. (f) Voltage-capacity plots of a Li-S cell with PPy modified separator under different current densities. (g) Rate performances of Li-S cells using different separators. (h) Cycling performances of a Li-S cell with high sulfur mass loading of 5.73 mg cm^{-2} using a PPy modified separator at 0.2 *C*.

morphology of Li metal anode and sulfur cathode after long-term cycling. The lithium metal electrode in the Li-S cell using a PPy modified separator exhibited a smooth surface, dense structure and preserved its structural integrity after 250 charge/discharge cycles (Fig. 5a and b, Fig. S10), suggesting uniform lithium stripping/plating behavior and good stability of lithium metal anode without obvious corrosion. At the cathode side, a clean surface was observed for the sulfur/carbon black cathode without residual solid sulfur species (Fig. 5c), indicating the good stability and reversibility of sulfur cathode. In comparison, the Li metal electrode in the Li-S cell with regular Celgard separator presented a rough surface, loose and porous structure with Li dendrites after cycling (Fig. 5d). Observed from the cross-sectional SEM image, the thickness of the loose and porous layer of "dead lithium" and accumulated SEI at the Li metal anode reached over 200 μm after 250 cycles (Fig. 5e), indicating the serious corrosion of lithium metal anode during cycling [37]. Moreover, solid deposits were observed on the surface of the sulfur/carbon black cathode (Fig. 5f), which may arise from the accumulated, inactive sulfur species due to the shuttling effect of intermediate polysulfides during extensive cycling [14,58]. The corrosion of lithium metal and undesired polysulfide shuttle effect affected the kinetics of the Li-S cell both at the anode and cathode side, consumed the electrolyte, and eventually led to the rapid degradation of battery performance (Fig. 6a). With an ultrathin PPy interfacial layer between the electrode and separator, the corrosion of lithium metal and shuttle effect of polysulfides are both suppressed, which enhanced the electrochemical performance of Li-S batteries (Fig. 6b).

3. Conclusion

In summary, we successfully engineered a stable electrode-separator interface with an ultrathin conductive polymer layer on the separator surface for practical high-energy-density Li-S batteries through a simple and scalable *in situ* vapor-phase polymerization approach. Such functional electrode-separator interface enhanced the electrolyte uptake, facilitated the uniform stripping/plating of Li metal, suppressed the polysulfide shuttle effect, and thus simultaneously improved the lithium metal anode and sulfur cathode in Li-S batteries. Consequently, with a PPy interfacial layer between the electrode and separator, the Li||Li symmetric cell delivered reduced polarization during the Li plating/stripping process in comparison to the bare counterpart. Using a PPy modified separator instead of a regular Celgard separator, a Li-S battery showed much improved electrochemical performance with only tiny increase in mass or volume based on the entire battery. The facile preparation of PPy interfacial layer and significant improvement in battery performance offer new insights into engineering functional electrode-separator interface for practical high-energy-density Li-S

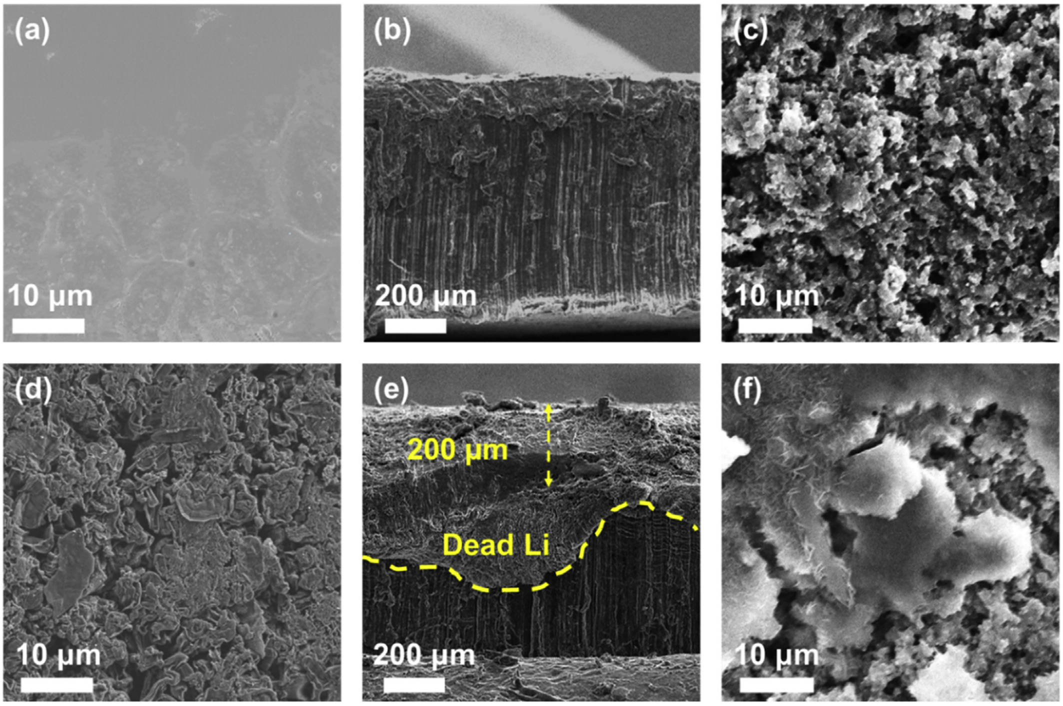

Fig. 5. (a) Top-view and (b) cross-section SEM images of Li metal anode and (c) top-view SEM image of sulfur cathode of the Li-S cells with PPy modified separators after 250 cycles at 0.5 *C*. (d) Top-view and (e) cross-section SEM images of Li metal anode and (f) top-view SEM image of sulfur cathode of the Li-S cells with regular Celgard separators after 250 cycles at 0.5 *C*.

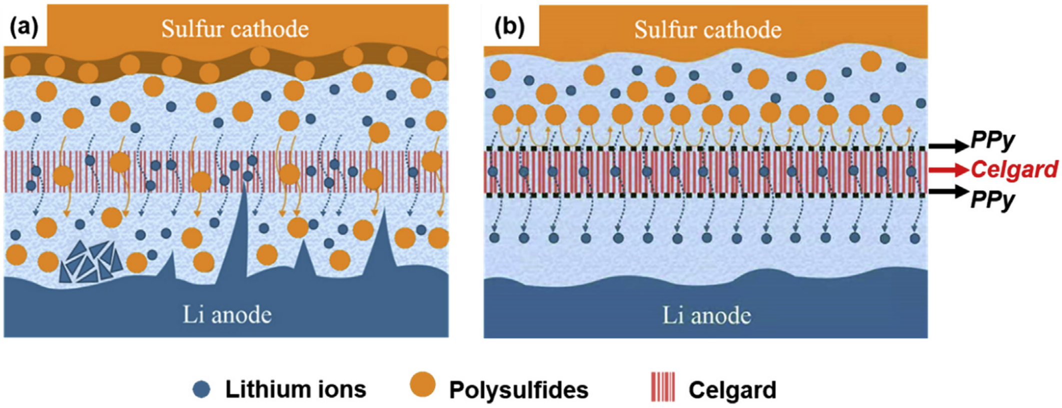

Fig. 6. Schematic illustration of the Li-S batteries with (a) a regular Celgard separator and (b) a PPy modified separator, respectively.

batteries.

4. Experimental section

4.1. Fabrication of polypyrrole (PPy)/Celgard separators

The PPy/Celgard separators were fabricated by a facile *in-situ* vapor-phase polymerization method. In detail, commercial Celgard separators were soaked into 0.1 mol L^{-1} $FeCl_3$ ethanol solution for 1 h and then were dried in ambient environment for 30 min. The treated Celgard separators and pyrrole monomer were placed in a sealed bottle and kept for 4 h. Finally, the PPy/Celgard separators were vacuum dried for overnight at 60 °C, cut into circular pieces and used for cell fabrication.

4.2. Preparation of sulfur/carbon black (S/CB) cathode

The impregnation of sulfur was carried out by mixing the CB power with sublimed sulfur in a 3:7 wt ratio. Then, the mixture was heated in a sealed glass bottle at 155 °C for 6 h. In order to prepare the slurry, S/CB composite was mixed with CB and PVDF (5 wt%) dissolved in anhydrous N-methyl-2-pyrrolidone. The weight ratio of S/CB composite, CB, and PVDF was 8:1:1, respectively. The slurry was casted onto an Al foil current collector and dried at 60 °C for 6 h in a vacuum oven, which resulted in the formation of S/CB cathode with a sulfur loading of 1.2 mg cm^{-2}.

4.3. Materials characterizations

The chemical compositions and morphologies of PPy/Celgard separators were analyzed using X-ray photoelectron spectroscopy (XPS, AXIS-ULTRA DLD-600W) and field emission SEM (FEI Nova Nano), respectively. For the SEM characterizations of electrodes after cycling, the electrodes were first extracted from the coin cells in the glove box and followed by gentle rinse with DOL to remove Li salt residue, and then were hermetically sealed inside an aluminum plastic bag for safe transfer.

4.4. Electrochemical measurements

All the electrochemical measurements were carried out with standard CR2032 coin-type cells assembled in the argon-filled glove box with the oxygen and water contents both below 0.1 ppm. The electrolyte was composed of 1 mol L^{-1} of LiTFSI in a mixture of DOL and DME (v/v = 1:1) with 0.2 mol L^{-1} of LiNO3. The Li||Li symmetric cells were primarily charged and discharged at 0–1 V (*vs.* Li/Li^+) at 0.1 mA cm^{-2} for five cycles for cell aging and activation. The areal capacity was fixed at 1 and 3 mAh cm^{-2} at a current density of 1 mA cm^{-2} for cycling. For the Li-S cells, the galvanostatic charge/discharge test were conducted from 1.7 V to 2.8 V (vs Li/Li^+) using a LAND 8-channel battery tester. The cyclic voltammetry (CV) and electrochemical impedance spectroscopy (EIS) measurements were carried out on a Biologic VMP3 system. The EIS tests were performed by applying an alternating current in the frequency range from 100 kHz to 0.01 Hz with 5 mV amplitude.

Acknowledgements

Z. W. S. thank the financial support from the Singapore National Research Foundation (NRF-NRFF2017-04). The authors would like to thank the Analytical and Testing Center of Huazhong University of Science and Technology as well as the Center for Nanoscale Characterization & Devices of Wuhan National Laboratory for Optoelectronics for providing the facilities to conduct the characterization.

Appendix A. Supplementary data

Supplementary data to this article can be found online at https://doi.org/10.1016/j.ensm.2019.05.005.

References

[1] K. Liu, Y.Y. Liu, D. Lin, Y. Cui, Sci. Adv. 4 (2018) eaas9820.
[2] M. Armand, J.M. Tarascon, Nature 451 (2008) 652.
[3] D. Lin, Y. Liu, Y. Cui, Nat. Nanotechnol. 12 (2017) 194–206.
[4] P.G. Bruce, S.A. Freunberger, L.J. Hardwick, J.M. Tarascon, Nat. Mater. 11 (2011) 19–29.
[5] Z.W. Seh, Y. Sun, Q. Zhang, Y. Cui, Chem. Soc. Rev. 45 (2016) 5605–5634.
[6] A. Manthiram, Y. Fu, S.H. Chung, C. Zu, Y.S. Su, Chem. Rev. 114 (2014) 11751–11787.
[7] F. Wu, J. Qian, R. Chen, T. Zhao, R. Xu, Y. Ye, W. Li, L. Li, J. Lu, K. Amine, Nano Energy 12 (2015) 742–749.
[8] Z. Li, J. Zhang, B. Guan, D. Wang, L.M. Liu, X.W. Lou, Nat. Commun. 7 (2016) 13065.
[9] H. Pan, J. Chen, R. Cao, V. Murugesan, N.N. Rajput, K.S. Han, K. Persson, L. Estevez, M.H. Engelhard, J.-G. Zhang, K.T. Mueller, Y. Cui, Y. Shao, J. Liu, Nat. Energy 2 (2017) 813–820.
[10] Y. Liu, Q. Liu, L. Xin, Y. Liu, F. Yang, E.A. Stach, J. Xie, Nat. Energy 2 (2017) 17083.
[11] R. Cao, J. Chen, K.S. Han, W. Xu, D. Mei, P. Bhattacharya, M.H. Engelhard, K.T. Mueller, J. Liu, J.-G. Zhang, Adv. Funct. Mater. 26 (2016) 3059–3066.
[12] J. Zhao, G. Zhou, K. Yan, J. Xie, Y. Li, L. Liao, Y. Jin, K. Liu, P.-C. Hsu, J. Wang, H.-M. Cheng, Y. Cui, Nat. Nanotechnol. 12 (2017) 993–999.
[13] Q. Pang, X. Liang, C.Y. Kwok, L.F. Nazar, Nat. Energy 1 (2016) 16132.
[14] Q. Pang, A. Shyamsunder, B. Narayanan, C.Y. Kwok, L.A. Curtiss, L.F. Nazar, Nat. Energy 3 (2018) 783–791.
[15] S. Bai, X. Liu, K. Zhu, S. Wu, H. Zhou, Nat. Energy 1 (2016) 16094.
[16] J.-Q. Huang, Q. Zhang, H.-J. Peng, X.-Y. Liu, W.-Z. Qian, F. Wei, Energy Environ. Sci. 7 (2014) 347–353.
[17] X. Ji, K.T. Lee, L.F. Nazar, Nat. Mater. 8 (2009) 500–506.
[18] G. Tan, R. Xu, Z. Xing, Y. Yuan, J. Lu, J. Wen, C. Liu, L. Ma, C. Zhan, Q. Liu, T. Wu, Z. Jian, R. Shahbazian-Yassar, Y. Ren, D.J. Miller, L.A. Curtiss, X. Ji, K. Amine, Nat. Energy 2 (2017) 17090.
[19] J.-Q. Huang, Q. Zhang, F. Wei, Energy Storage Mater. 1 (2015) 127–145.
[20] L. Fan, M. Li, X. Li, W. Xiao, Z. Chen, J. Lu, Joule 3 (2019) 1–26.
[21] Y. Pan, S. Chou, H.K. Liu, S.X. Dou, Natl. Sci. Rev. 4 (2017) 917–933.
[22] J. Balach, T. Jaumann, M. Klose, S. Oswald, J. Eckert, L. Giebeler, Adv. Funct. Mater. 25 (2015) 5285–5291.
[23] S. Tu, X. Chen, X. Zhao, M. Cheng, P. Xiong, Y. He, Q. Zhang, Y. Xu, Adv. Mater. 30 (2018) 1804581.
[24] S.-H. Chung, A. Manthiram, Adv. Funct. Mater. 24 (2014) 5299–5306.
[25] S. Niu, W. Lv, G. Zhou, H. Shi, X. Qin, C. Zheng, T. Zhou, C. Luo, Y. Deng, B. Li, F. Kang, Q.-H. Yang, Nano Energy 30 (2016) 138–145.
[26] G. Ma, F. Huang, Z. Wen, Q. Wang, X. Hong, J. Jin, X. Wu, J. Mater. Chem. A 4 (2016) 16986.
[27] L. Kong, B.-Q. Li, H.-J. Peng, R. Zhang, J. Xie, J.-Q. Huang, Q. Zhang, Adv. Energy Mater. 20 (2018) 1800849.
[28] Z.A. Ghazi, X. He, A.M. Khattak, N.A. Khan, B. Liang, A. Iqbal, J. Wang, H. Sin, L. Li, Z. Tang, Adv. Mater. 29 (2017) 1606817.
[29] J. He, Y. Chen, A. Manthiram, Energy Environ. Sci. 11 (2018) 2560–2568.
[30] T. Zhou, W. Lv, J. Li, G. Zhou, Y. Zhao, S. Fan, B. Liu, B. Li, F. Kang, Q.-H. Yang, Energy Environ. Sci. 10 (2017) 1694–1703.
[31] H.J. Peng, Z.W. Zhang, J.Q. Huang, G. Zhang, J. Xie, W.T. Xu, J.L. Shi, X. Chen, X.B. Cheng, Q. Zhang, Adv. Mater. 28 (2016) 9551–9558.
[32] F. Wu, S. Zhao, L. Chen, Y. Lu, Y. Su, Y. Jia, L. Bao, J. Wang, S. Chen, R. Chen, Energy Storage Mater. 14 (2018) 383–391.
[33] Z. Xiao, Z. Yang, L. Wang, H. Nie, M. Zhong, Q. Lai, X. Xu, L. Zhang, S. Huang, Adv. Mater. 27 (2015) 2891–2898.
[34] Y.S. Su, A. Manthiram, Nat. Commun. 3 (2012) 1166.
[35] H. Yao, K. Yan, W. Li, G. Zheng, D. Kong, Z.W. Seh, V.K. Narasimhan, Z. Liang, Y. Cui, Energy Environ. Sci. 7 (2014) 3381–3390.
[36] H. Lee, X. Ren, C. Niu, L. Yu, M.H. Engelhard, I. Cho, M.-H. Ryou, H.S. Jin, H.-T. Kim, J. Liu, W. Xu, J.-G. Zhang, Adv. Funct. Mater. 27 (2017) 1704391.
[37] R. Pan, X. Xu, R. Sun, Z. Wang, J. Lindh, K. Edstrom, M. Stromme, L. Nyholm, Small 14 (2018) 1704371.
[38] M.-H. Ryou, D.J. Lee, J.-N. Lee, Y.M. Lee, J.-K. Park, J.W. Choi, Adv. Energy Mater. 2 (2012) 645–650.
[39] Y. He, Z. Chang, S. Wu, Y. Qiao, S. Bai, K. Jiang, P. He, H. Zhou, Adv. Energy Mater. 8 (2018) 1802130.
[40] J. Wu, H. Zeng, X. Li, X. Xiang, Y. Liao, Z. Xue, Y. Ye, X. Xie, Adv. Energy Mater. 8 (2018) 1802430.
[41] N. Zhang, B. Li, S. Li, S. Yang, Adv. Energy Mater. 8 (2018) 1703124.
[42] J. Sun, Y. Sun, M. Pasta, G. Zhou, Y. Li, W. Liu, F. Xiong, Y. Cui, Adv. Mater. 28 (2016) 9797–9803.
[43] F. Pei, L. Lin, A. Fu, S. Mo, D. Ou, X. Fang, N. Zheng, Joule 2 (2018) 323–336.
[44] P.J.H. Kim, J. Seo, K. Fu, J. Choi, Z. Liu, J. Kwon, L. Hu, U. Paik, NPG Asia Mater. 9 (2017) e375-e375.
[45] X. Fu, Y. Wang, L. Scudiero, W.-H. Zhong, Energy Storage Mater. 15 (2018) 447–457.
[46] L. Wang, Y.-B. He, L. Shen, D. Lei, J. Ma, H. Ye, K. Shi, B. Li, F. Kang, Nano Energy 50 (2018) 367–375.
[47] L.B. Wang, X.X. Liu, R. Zeng, M. Li, Y.H. Huang, X.L. Hu, Angew. Chem. 129 (2017) 1125–1130.
[48] J.X. Feng, H. Xu, S.H. Ye, G. Ouyang, Y.X. Tong, G.R. Li, Angew. Chem. 56 (2017) 8120–8124.
[49] W. Li, Q. Zhang, G. Zheng, Z.W. Seh, H. Yao, Y. Cui, Nano Lett. 13 (2013) 5534–5540.
[50] L. Kong, B.-Q. Li, H.-J. Peng, R. Zhang, J. Xie, J.-Q. Huang, Q. Zhang, Adv. Energy Mater. 20 (2018) 1800849.
[51] M. Yoshio, R.J. Brodd, A. Kozawa, Lithium-Ion Batteries Science and Technologies, Springer, New York, 2009, pp. 183–185.
[52] Z. Wang, R. Pan, C. Xu, C. Ruan, K. Edström, M. Strømme, L. Nyholm, Energy Storage Mater. 13 (2018) 283–292.
[53] P. Han, S.-H. Chung, A. Manthiram, Energy Storage Mater. 17 (2019) 317–324.
[54] F. Li, M.R. Kaiser, J. Ma, Z. Guo, H. Liu, J. Wang, Energy Storage Mater. 13 (2018) 312–322.
[55] K. Shi, C. Lai, X. Liu, Y. Wei, W. Lv, J. Wang, J. Li, C. Yan, B. Li, Q.-H. Yang, F. Kang, Y.-B. He, Energy Storage Mater. 17 (2019) 111–117.
[56] J.-Q. Huang, T.-Z. Zhuang, Q. Zhang, H.-J. Peng, C.-M. Chen, F. Wei, ACS Nano 9 (2015) 3002–3011.
[57] H. Lee, H. Lim, X. Ren, L. Yu, M.H. Engelhard, K. Han, J. Lee, H.-T. Kim, Kim, J. Xiao, J. Liu, W. Xu, J.-G. Zhang, ACS Energy Lett. 3 (2018) 2921–2930.
[58] Y. Tsao, M. Lee, E.C. Miller, G. Gao, J. Park, S. Chen, T. Katsumata, H. Tran, L.-W. Wang, M.F. Toney, Y. Cui, Z. Bao, Joule 3 (2019) 1–13.